JOURNAL OF MATERIALS SCIENCE **40** (2005) 1183–1191

# Research on the interaction of three contact fibers in the fiber suspensions

JIANZHONG LIN*, XIAOCHUAN CHAI
*Department of Mechanics, State Key Laboratory of Fluid Power Transmission and Control, Zhejiang University, Hangzhou 310027, People's Republic of China*
*E-mail: mecjzlin@yahoo.com*

JAMES A. OLSEN
*Department of Mechanical Engineering, Pulp and Paper Center, The University of British Columbia, Vancouver, BC, Canada V6T 1Z4*

Based on the slender-body theory, the governing equations for the mechanical interaction of one settling fiber with two fixed fibers in fiber suspensions were derived and solved numerically. In order to validate the model and method used in the paper, the interactions of two contact fibers were simulated and the results are in good accordance with the experiments. The results of three interacting fibers show that the initial contact point and the initial orientation angle of settling fiber have a significant effect, however, the angle between two fixed fibers has an insignificant effect, and the initial angular velocity of settling fiber has no effect on the interaction process of fibers. The settling fiber aspect ratio is not an independent parameter involving in the interaction between the fibers. The interaction duration increases as the fiber aspect ratio increases, however, the effect caused by reducing the diameter is more significant than that caused by increasing the length. The interaction duration is directly proportional to the solvent viscosity and verse directly to the fiber specific weight remarkably. Finally, a synthetic parameter $A$ which contains the quantities affecting the interaction duration is derived to uniquely describe the total duration of interaction of the fibers. 

## Nomenclature

| | |
|---|---|
| $a_n$ | axial acceleration of the contact point (m s$^{-2}$) |
| $a_t$ | transverse acceleration of the contact point (m s$^{-2}$) |
| $a_\varepsilon$ | relative acceleration of the center to the contact point, equals to $as$(m s$^{-2}$) |
| $A$ | synthetic parameter |
| $\boldsymbol{F}(s)$ | line density of the Stokes force acting on the fluid by a fiber (kg s$^{-2}$) |
| $\boldsymbol{F}_c$ | contact force (N) |
| $F_n$ | normal component of contact force (N) |
| $F_t$ | tangential component of contact force (N) |
| $F_x$ | tangential component of the Stokes force (N) |
| $F_y$ | normal component of the Stokes force (N) |
| $G$ | difference of gravitation and buoyancy (N) |
| $I$ | moment of inertia about the fiber center (kg m$^2$) |
| $l$ | half length of fiber (m) |
| $L$ | length of fiber (m) |
| $l_0$ | characteristic length of fiber (m) |
| $M$ | torque acting on the fiber (kg m$^2$ s$^{-2}$) |
| $m$ | mass of fiber (kg) |
| $\boldsymbol{n}$ | a unit vector normal to fibers |
| $\boldsymbol{p}$ | orientation of fiber, a unit vector |
| $P_x$ | component of $\boldsymbol{p}$, equals to $\cos\theta$ |
| $R$ | radius of fiber (m) |
| $R_o$ | radius at the fiber center (m) |
| $R_s$ | radius of fiber at position $s$ (m) |
| $R_0$ | characteristic radius of fiber (m) |
| $s$ | distance from any position to the center of settling fiber (m) |
| $s^*$ | dimensionless form of $s$, $s^* = s/l$ |
| $S$ | distance from the center of settling fiber to the contact point (m) |
| $S_c$ | position of contact point (m) |
| $S_0$ | position of initial contact point (m) |
| $\boldsymbol{v}$ | velocity at contact point (m s$^{-1}$) |
| $\boldsymbol{v}_o$ | translational velocity of the fiber (m s$^{-1}$) |
| $\boldsymbol{v}_{\text{induce}}$ | induced velocity by fixed fiber (m s$^{-1}$) |
| $\boldsymbol{v}^\infty$ | undisturbed velocity at $\boldsymbol{x}$ (m s$^{-1}$) |
| $\boldsymbol{x}$ | vector of position (m) |
| $\boldsymbol{x}_0$ | position of fiber center (m) |
| $\boldsymbol{\delta}$ | Kronecker operator |
| $\varepsilon$ | a quantity equals to $[\log(2l/R_o)]^{-1}$ |
| $\eta$ | coefficient of drag |
| $\theta$ | angle between fiber axis and horizontal (o) |
| $\dot{\theta}$ | angular velocity of settling fiber (o s$^{-1}$) |
| $\ddot{\theta}$ | angular acceleration of settling fiber (o s$^{-2}$) |

*Author to whom all correspondence should be addressed.

| | |
|---|---|
| $\theta_0$ | initial angle between fiber axis and horizontal (o) |
| $\mu$ | solvent dynamic viscosity (kg m$^{-1}$ s$^{-1}$) |
| $\nu$ | solvent kinematic viscosity (m$^2$ s$^{-1}$) |
| $\nu_0$ | characteristic solvent viscosity (m$^2$ s$^{-1}$) |
| $\rho$ | fiber specific weight (kg m$^{-3}$) |
| $\rho_0$ | characteristic fiber specific weight (kg m$^{-3}$) |
| $\varphi$ | fiber aspect ratio |
| $\mathbf{\Omega}$ | vector of angular velocity of fiber (o s$^{-1}$) |

## Subscript

| | |
|---|---|
| $c$ | contact point |
| 1 | fiber 1 |
| 2 | fiber 2 |
| 3 | fiber 3 |

## 1. Introduction

The investigation of fiber suspension has attracted considerable attention due to their numerous industrial and practical applications. In the material science, the behavior of short fibers immersed in a viscous fluid is an important problem in the processing of composite materials. The strength and stiffness of composite material depend on the orientation of fiber. When fiber concentration is high enough, the interactions between fibers have a significant effect on the microstructure of a suspension, and hence on its macroscopic properties such as enhancement of effective viscosity, finite normal stress differences [2], yield stress [3], rod climbing [4] and shear thinning.

One of the important interactions of fibers is mechanical contact between fibers. There are some studies devoted to this topic. Andersson and Rasmuson [5] investigated experimentally the friction of pulp and synthetic fibers in both air and water, and found that the sliding fiber alternately sticks and slides as it was pulled upward. Modifications of the classical, single-parameter law relating frictional resistance to normal force were given to improve agreement with experimental results. Stick-slide behavior and deviations from classical friction laws were also found by Lee [6] in measurements of interfacial shear strength of 25–35 $\mu$m diameter silica fibers. Zeng *et al.* [7] determined the friction coefficient governing contact between a sedimenting sphere and a neutrally buoyant sphere. Petrich and Koch [8] studied the nature of the forces involved in mechanical contact between fibers in a fluid and the interaction between a polymeric fiber settling under the influence of gravity and a fixed strand of the same material, and the static coefficient of friction was found to be $0.38 \pm 0.06$. Chaouche and Koch [9] examined the influence of adhesive contacts between fibers on rheology of suspension. Lin *et al.* [10] constructed a mathematical model for the mechanical interactions between two contact fibers, based on which numerical simulations were performed. The results show that settling fiber begins to slide at earlier time and the entire interaction duration diminishes as the initial position of the contact point, the initial orientation of fiber and the fiber specific weight increase or the solvent viscosity decreases.

Related to the interactions of fibers, the process and duration of interactions are crucial. Therefore, it is necessary to investigate the factors affecting the process and duration of interactions. The factors include the initial contact point, initial orientation and angular velocity of settling fiber, the fiber aspect ratio and specific weight, the solvent viscosity. It is especially meaningful to generalize a synthetic parameter to describe the total interaction duration of the fibers. In spite of the experimental and theoretical results for the interaction of two fibers, the interactions of three fibers are still not well understood and have not been reported yet. The aim of this study is to derive a set of governing equations for the mechanical interaction of three contact fibers, shed light on the effects of factors mentioned above on the interactions of the fibers, and generalize a synthetic parameter to describe the interaction duration of the fibers by performing numerical simulations.

## 2. Governing equation

There are many situations for three contact fibers. The situation studied in this paper is shown in Fig. 1. Fiber 2 and fiber 3 are horizontally fixed and fiber 1 falls from a very short distance above the fixed fibers. The

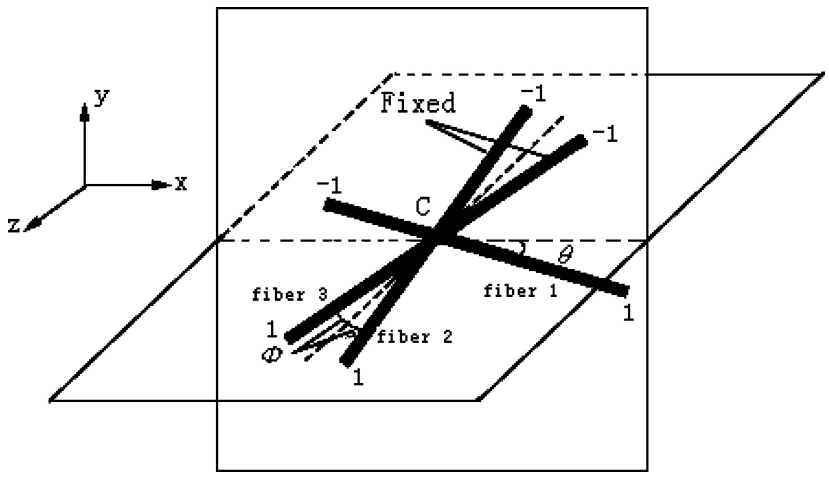


*Figure 1* Sketch of three contact fibers.

track of settling fiber can be represented by the evolution of $P_x$ and $S_c$. The orientation of settling fiber is denoted by the unit vector $\boldsymbol{p}$. After contacting, the settling fiber pivots about the initial contact point. The fiber rotates in this manner until the tangential component of the gravitational force overcame static friction, so that the fiber starts to slide along the fixed fiber while rotating.

The Reynolds number for the motion of settling fiber is very small (less than $1 \times 10^{-3}$). Therefore, the inertial can be neglected and the forces imposed on the settling fiber are assumed to be gravity, hydrodynamic drag, long-range disturbance force caused by the fixed fibers, and contact force $\boldsymbol{F}_c$ which prevents the fibers from penetrating each other and provides a frictional resistance to the sliding motion.

Based on the slender-body theory [11], the velocity at the surface of a fiber is the superposition of the fluid's undisturbed velocity and the disturbed velocity due to the presence of other fibers. Thus, for an isolated fiber, we have [12]:

$$\begin{aligned}
&\boldsymbol{v}_o + \boldsymbol{\Omega} \times ls^*\boldsymbol{p}] \\
&= \boldsymbol{v}_{\text{induce}}(\mathbf{x}_o + ls^*\boldsymbol{p}) + \boldsymbol{v}^{\infty}(\mathbf{x}_o + ls * \boldsymbol{p}) \\
&= \frac{1}{4\pi\mu}\left(\frac{1}{\varepsilon} + \ln\frac{\left(1-s^{*2}\right)^{\frac{1}{2}}}{R_s/R_0}\right)(\delta + \boldsymbol{p}\boldsymbol{p}) \cdot \boldsymbol{F}(ls^*) \\
&\quad + \frac{1}{8\pi\mu}(\delta - 3\boldsymbol{p}\boldsymbol{p}) \cdot \boldsymbol{F}(ls^*) + \frac{1}{8\pi\mu}(\delta + \boldsymbol{p}\,p) \\
&\quad \cdot \int_{-1}^{1} \frac{\boldsymbol{F}(s^{*\prime}) - \boldsymbol{F}(s^*)}{|s^* - s^{*\prime}|} ds^{*\prime} + \boldsymbol{v}^{\infty}(\boldsymbol{x}_o + ls^*\boldsymbol{p}) \quad (1)
\end{aligned}$$

where the dot operator "·" stands for the scalar product, the square bracket [ ] is a vector-vector function.

The line density of the Stokes force acting on the fluid by the fiber, $\boldsymbol{F}(s^*)$, can be then solved from Equation 1. However, the presence of the horizontally fixed fibers will give rise to additional disturbed velocity, hence we need to combine the integral equations of the three fibers as follows:

$$\begin{aligned}
&\boldsymbol{v}_{o1} + [\boldsymbol{\Omega}_1 \times ls_1^*\boldsymbol{p}_1] \\
&= \frac{1}{4\pi\mu}\left(\frac{1}{\varepsilon} + \ln\frac{\left(1-s_1^{*2}\right)^{\frac{1}{2}}}{R_s/R_0}\right)(\boldsymbol{\delta} + \boldsymbol{p}_1\boldsymbol{p}_1) \cdot \boldsymbol{F}_1(ls_1^*) \\
&\quad + \frac{1}{8\pi\mu}(\boldsymbol{\delta} - 3\boldsymbol{p}_1\boldsymbol{p}_1) \cdot \boldsymbol{F}_1(ls_1^*) \\
&\quad + \frac{1}{8\pi\mu}(\boldsymbol{\delta} + \boldsymbol{p}_1\boldsymbol{p}_1) \cdot \int_{-1}^{1} \frac{\boldsymbol{F}_1(ls_1^{*\prime}) - \boldsymbol{F}_1(ls_1^*)}{|s_1^* - s_1^{*\prime}|} ds_1^{*\prime} \\
&\quad + \int_{-1}^{1} \boldsymbol{H}(\boldsymbol{x}_{o1} + s_1\boldsymbol{p}_1 - \boldsymbol{x}_{o2} - s_2\boldsymbol{p}_2) \cdot \boldsymbol{F}_2(ls_2^*)\, ds_2^* \\
&\quad + \int_{-1}^{1} \boldsymbol{H}(\boldsymbol{x}_{o1} + s_1\boldsymbol{p}_1 - \boldsymbol{x}_{o3} - s_3\boldsymbol{p}_3) \cdot \boldsymbol{F}_3(ls_3^*)\, ds_3^* \\
&\quad + \boldsymbol{v}^{\infty}(\boldsymbol{x}_{o1} + ls_1^*\boldsymbol{p}_1)
\end{aligned}$$

$$\begin{aligned}
&\boldsymbol{v}_{o2} + [\boldsymbol{\Omega}_2 \times ls_2^*\boldsymbol{p}_2] \\
&= \frac{1}{4\pi\mu}\left(\frac{1}{\varepsilon} + \ln\frac{\left(1-s_2^{*2}\right)^{\frac{1}{2}}}{R_s/R_0}\right)(\boldsymbol{\delta} + \boldsymbol{p}_2\boldsymbol{p}_2) \cdot \boldsymbol{F}_2(ls_2^*) \\
&\quad + \frac{1}{8\pi\mu}(\boldsymbol{\delta} - 3\boldsymbol{p}_2\boldsymbol{p}_2) \cdot \boldsymbol{F}_2(ls_2^*) \\
&\quad + \frac{1}{8\pi\mu}(\boldsymbol{\delta} + \boldsymbol{p}_2\boldsymbol{p}_2) \cdot \int_{-1}^{1} \frac{\boldsymbol{F}_2(ls_2^{*\prime}) - \boldsymbol{F}_2(ls_2^*)}{|s_2^* - s_2^{*\prime}|} ds_2^* \\
&\quad + \int_{-1}^{1} \boldsymbol{H}(\boldsymbol{x}_{o2} + s_2\boldsymbol{p}_2 - \boldsymbol{x}_{o1} - s_1\boldsymbol{p}_1) \cdot \boldsymbol{F}_1(ls_1^*)\, ds_1^* \\
&\quad + \int_{-1}^{1} \boldsymbol{H}(\boldsymbol{x}_{o2} + s_2\boldsymbol{p}_2 - \boldsymbol{x}_{o3} - s_3\boldsymbol{p}_3) \cdot \boldsymbol{F}_3(ls_3^*)\, ds_3^* \\
&\quad + \boldsymbol{v}^{\infty}(\boldsymbol{x}_{o2} + ls_2^*\boldsymbol{p}_2)
\end{aligned}$$

$$\begin{aligned}
&\boldsymbol{v}_{o3} + [\boldsymbol{\Omega}_3 \times ls_3^*\boldsymbol{p}_3] \\
&= \frac{1}{4\pi\mu}\left(\frac{1}{\varepsilon} + \ln\frac{\left(1-s_3^{*2}\right)^{\frac{1}{2}}}{R_s/R_0}\right)(\boldsymbol{\delta} + \boldsymbol{p}_3\boldsymbol{p}_3) \cdot \boldsymbol{F}_3(ls_3^*) \\
&\quad + \frac{1}{8\pi\mu}(\boldsymbol{\delta} - 3\boldsymbol{p}_3\boldsymbol{p}_3) \cdot \boldsymbol{F}_3(ls_3^*) \\
&\quad + \frac{1}{8\pi\mu}(\boldsymbol{\delta} + \boldsymbol{p}_3\boldsymbol{p}_3) \cdot \int_{-1}^{1} \frac{\boldsymbol{F}_3(ls_3^{*\prime}) - \boldsymbol{F}_3(ls_3^*)}{|s_3^* - s_3^{*\prime}|} ds_3^* \\
&\quad + \int_{-1}^{1} \boldsymbol{H}(\boldsymbol{x}_{o3} + s_3\boldsymbol{p}_3 - \boldsymbol{x}_{o1} - s_1\boldsymbol{p}_1) \cdot \boldsymbol{F}_1(ls_1^*)\, ds_1^* \\
&\quad + \int_{-1}^{1} \boldsymbol{H}(\boldsymbol{x}_{o3} + s_3\boldsymbol{p}_3 - \boldsymbol{x}_{o2} - s_2\boldsymbol{p}_2) \cdot \boldsymbol{F}_2(ls_2^*)\, ds_2^* \\
&\quad + \boldsymbol{v}^{\infty}(\boldsymbol{x}_{o3} + ls_3^*\boldsymbol{p}_3) \qquad (2)
\end{aligned}$$

where H is a tensor function:

$$\boldsymbol{H}(\boldsymbol{x}) = \frac{1}{8\pi\mu}\left(\frac{\boldsymbol{\delta}}{|\boldsymbol{x}|} + \frac{\boldsymbol{x}x}{|\boldsymbol{x}|^3}\right)$$

After taking discretion to Equation 2 by Gauss-Legendre integral formulation, we obtain a set of linear algebra equations for the densities of the Stokes force on all Gauss points. By integrating these discrete forces, the resultant Stokes force as well as a torque about the center can be obtained. We focus on the motion of the settling fiber, so the resultant force exerted on the settling fiber can be decomposed into a tangential component $F_x$ and a normal component $F_y$.

The settling fiber experiences two different stages after touching the fixed fibers. Firstly, it only pivots about the fixed fiber and secondly, it slides along the fixed fiber while rotating about it.

Fig. 2 shows the motion of the settling fiber and all forces on it in the first stage. $F_x$, $F_y$ and $M$ can be obtained through Gauss numerical integration method demonstrated above.

The dynamic equations of the settling fiber area:

$$\left.\begin{aligned}
G\sin\theta + F_x - F_t &= -m\dot{\theta}^2 s \\
G\cos\theta - F_y - F_n &= m\ddot{\theta}s \\
M + F_n s &= I\ddot{\theta}
\end{aligned}\right\} \qquad (3)$$

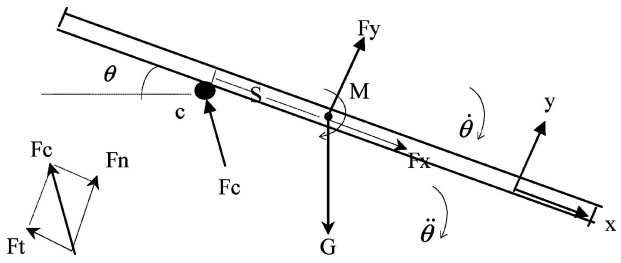


*Figure 2* The motion of fiber and forces acting on the fiber in the first stage.

where $I = mR^2/4 + ml^2/3$. Solving Equation 3, we have

$$\begin{cases} \ddot{\theta} = (G\cos\theta \cdot s + M - F_y s)/(I + ms^2) \\ F_n = G\cos\theta \dfrac{I}{I + ms^2} - F_y - \dfrac{(ms \cdot M - mF_y s^2)}{I + ms^2} \\ F_t = G\sin\theta + m\dot{\theta}^2 s + F_x \end{cases} \tag{4}$$

In Equation 4 we can judge whether the settling fiber will begin to slide from the values of $F_n$ and $F_t$.

Figs 3 and 4 show the settling fiber motion condition in the second stage and all forces on the fiber, respectively. The fiber dynamic equations are as follows:

$$\left.\begin{array}{c} G\sin\theta + F_x - F_t = m(a_t - \dot{\theta}^2 s) \\ G\cos\theta - F_y - F_n = m(a_n + \ddot{\theta} \cdot s) \\ M + F_n s = I\ddot{\theta} \end{array}\right\} \tag{5}$$

There are five variables but only three equations in Equation 5. We need two additional equations, one of

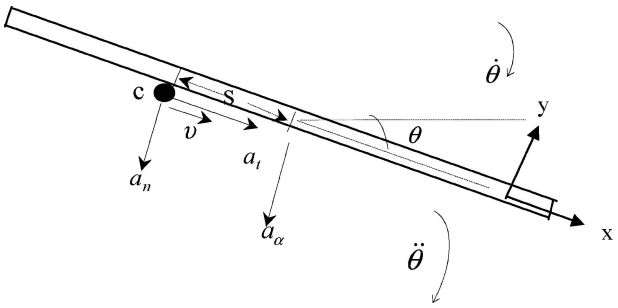


*Figure 3* The motion of the settling fiber in the second stage.

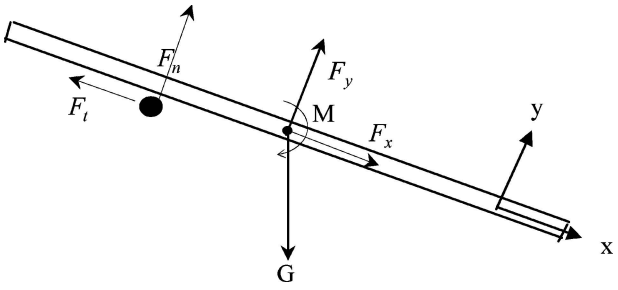


*Figure 4* The forces on the settling fiber in the second stage.

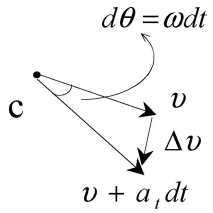


*Figure 5* The variation of settling fiber velocity at contact point *c*.

which is the frictional equation [10]:

$$F_t = \mu F_n + F_0 + \eta\upsilon \tag{6}$$

The third term on the right hand of Equation 6 is additional drag, which accounts for the finite transverse dimension of the fiber and lubrication interactions between fibers. The coefficient $\eta$ is $3.0 \times 10^{-4}$ in this paper based on the experimental results [8]. Another additional equation can be obtained by analyzing the variation of fiber velocity at contact point $c$ during a very small time step $dt$. From Fig. 5 we can get an approximate formulation for its transverse acceleration:

$$a_n = \upsilon\dot{\theta} \tag{7}$$

Combining Equations 5–7, we can determine $\ddot{\theta}$ and $a_t$:

$$\begin{cases} \ddot{\theta} = (G\cos\theta - m\dot{\theta}\upsilon - F_y + M/s)/(I/s + ms) \\ a_t = (G\sin\theta + F_x + m\dot{\theta}^2 s - \mu(\mathrm{I}\ddot{\theta} - M)/s \\ \qquad -F_0 - \eta\upsilon)/m \end{cases} \tag{8}$$

Once the initial contact position and angular velocity of the settling fiber are given, we can determine the settling fiber motion at any time, including its velocity and displacement. In order to validate the model and method used in the paper, the interactions of two contact fibers were simulated and compared with the experiments. Fig. 6 shows the results, in which the solid lines represent the numerical results and the symbols $\circ(P_y)$ and $\times(S_c)$ represent the experimental results [8].

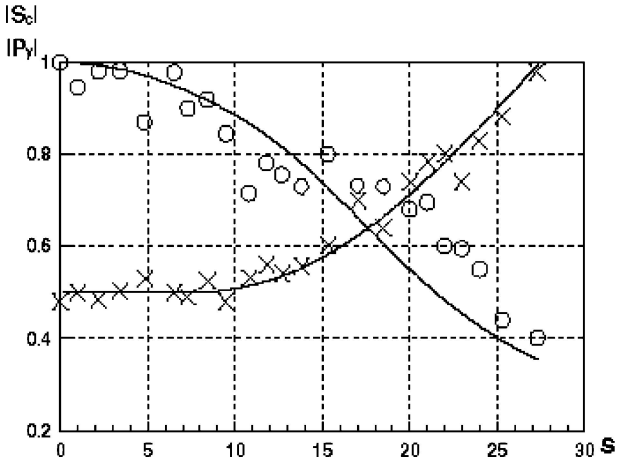


*Figure 6* Comparison of the calculated results with the experiment ones [8].

The fiber used in the experiments is cellulose acetate propionate with the length of 3 mm and the diameter of 80 $\mu$m and the density of 1.222 $\times 10^3$ kg/m$^3$. The fluid is silicon oil with the viscosity of 20 cSt and the density of 0.95 $\times$ $10^3$ kg/m$^3$. We can see that both results are agreeable.

## 3. Results and discussions

### 3.1. Effect of initial contact point on the process of interaction

Fig. 7a depicts the variation of position of contact point with time at different initial contact points $S_0$. Table I lists the time when settling fiber starts sliding along and departs the fixed fiber at different initial contact points $S_0$, respectively. We see that the settling fiber begins to slide at earlier time and the interaction duration between settling fiber and fixed fiber decreases as $S_0$ increases. Fig. 7b shows that the angle between settling fiber axis and horizontal ($P_x = \cos\theta$) turns large quickly for the situations with large $S_0$.

TABLE I The time when settling fiber starts sliding along and departs the fixed fiber at different $S_0$

| $S_0$ (mm) | 0.05 $l$ | 0.10 $l$ | 0.15 $l$ | 0.20 $l$ | 0.25 $l$ | 0.30 $l$ |
|---|---|---|---|---|---|---|
| Time of start sliding (s) | 21.5 | 10.75 | 7.16 | 5.37 | 4.3 | 4.59 |
| Time of departing fixed fiber (s) | 44.43 | 29.15 | 23.07 | 19.64 | 17.37 | 15.72 |

TABLE II The time when settling fiber starts sliding along and departs the fixed fiber at different $\theta_0$

| $\theta_0$ (o) | 0 | 10 | 15 | 20 | 25 | 30 |
|---|---|---|---|---|---|---|
| Time of start sliding (s) | 5.37 | 2.62 | 1.21 | 0 | 0 | 0 |
| Time of departing fixed fiber (s) | 19.64 | 16.89 | 15.48 | 14.05 | 12.74 | 12.60 |

### 3.2. Effect of initial orientation of settling fiber on the process of interaction

For different initial angles $\theta_0$ between settling fiber axis and horizontal, the position of contact point and angle between settling fiber axis and horizontal at different time are shown in Fig. 8. The time when settling fiber starts sliding along and departs the fixed fiber at different initial orientation $\theta_0$ of settling fiber is listed in Table II. From the figure and table it is found that the interaction duration between settling fiber and fixed fiber becomes short with increasing of initial angles between two kinds of fibers. When the initial angles are within 15°–20°, the settling fiber does not pivot about the fixed fiber, while sliding along and rotating the fixed fiber directly.

### 3.3. Effect of angle between two fixed fibers on the process of interaction

Fig. 9 shows the position of contact point and angle between settling fiber axis and horizontal at different time for different angle $\phi$ between two fixed fibers. Table III gives the time when settling fiber starts sliding along and departs the fixed fiber at different $\phi$, respectively. It can be seen that $\phi$ has an infinitesimal effect on the $S_0$

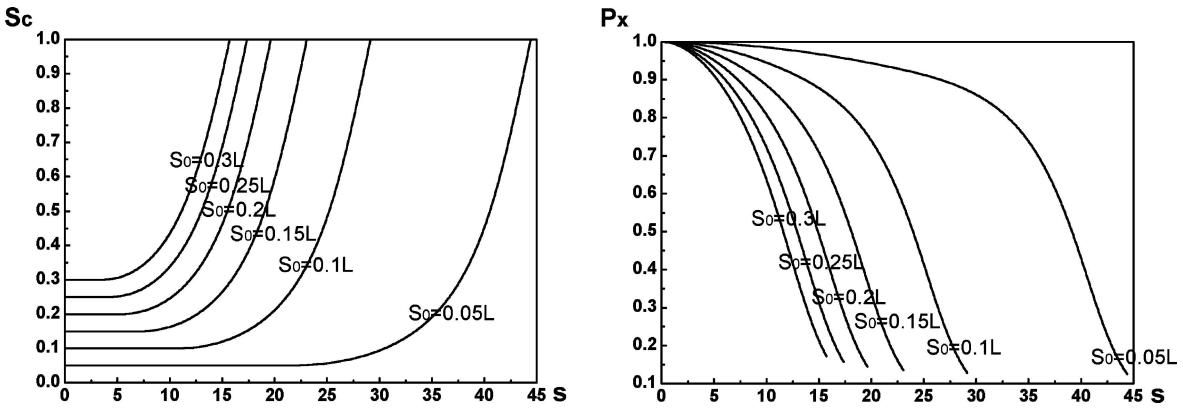


*Figure 7* The results for the different initial contact points of fibers (the unit of $S_0$ is mm).

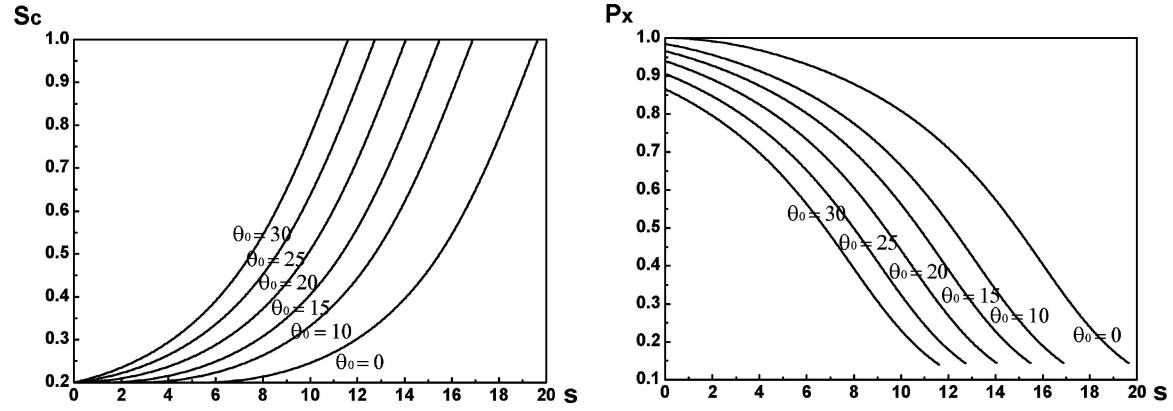


*Figure 8* The results for different initial orientation of settling fiber (the unit of $\theta_0$ is o).

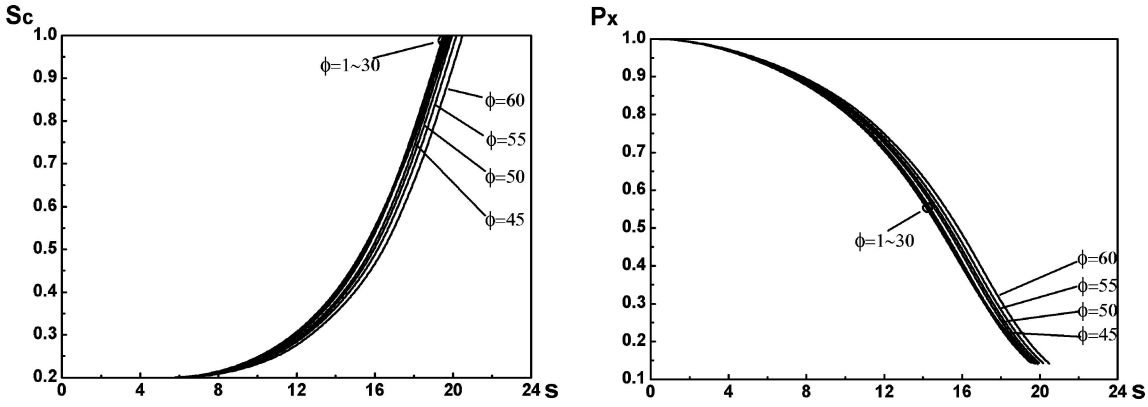


*Figure 9* The results for different angle $\phi$ (the unit of $\phi$ is o).

and $P_x$ when $\phi$ is less than 30°. When $\phi$ is larger than 30°, the settling fiber begins to slide at later time and the interaction duration between settling fiber and fixed fiber increases as $\phi$ increases. There exists a minimum, which is around 20°, for the time when the settling fiber departs from the fixed fiber. As for the time when the settling fiber starts sliding, the values change a little when $\phi$ is less than 30° and increase obviously when $\phi$ is larger than 30°.

## 3.4. Effect of initial angular velocity of settling fiber on the process of interaction

We perform computation with eight different initial angular velocities of settling fiber (i.e. 0, 3, 5, 10, 20, 30, 40, 50 °/s) , the eight curves overlap as shown in Fig. 10. It indicates that the initial angular velocity of settling fiber has no effect on the position of contact point and the angle between settling fiber axis and horizontal.

## 3.5. Effect of fiber aspect ratio on the process of interaction

Different fiber aspect ratios $\varphi = l/R$ can be determined by changing the fiber diameter or length. The results obtained by changing fiber length at the fixed radius $R = 40\ \mu$m are depicted in Fig. 11 and those obtained by varying the fiber diameter at the fixed length $2l = 3$ mm are shown in Fig. 12. Table IV lists the angles between the settling fiber and fixed fiber when the settling fiber departs the fixed fiber and the time when the settling fiber starts sliding along and departs the fixed fiber at different fiber aspect ratio, in which $\varphi_l$

TABLE III The time when settling fiber starts sliding along and departs the fixed fiber at different $\phi$

| $\phi$ (o) | 3 | 5 | 10 | 15 | 18 | 20 |
|---|---|---|---|---|---|---|
| Time of start sliding (s) | 5.34 | 5.35 | 5.37 | 5.36 | 5.36 | 5.37 |
| Time of departing fixed fiber (s) | 19.75 | 19.70 | 19.64 | 19.56 | 19.54 | 19.53 |
| $\phi$(o) | 25 | 30 | 45 | 50 | 55 | 60 |
| Time of start sliding (s) | 5.38 | 5.39 | 5.47 | 5.51 | 5.56 | 5.63 |
| Time of departing fixed fiber (s) | 19.54 | 19.57 | 19.80 | 19.95 | 20.17 | 20.48 |

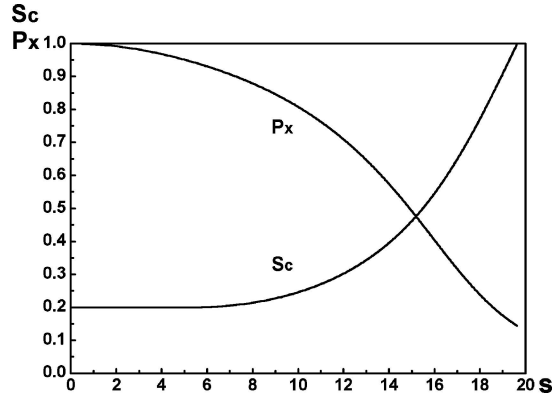


*Figure 10* The results for different initial angular velocity of settling fiber.

and $\varphi_r$ represent aspect ratio when changing the fiber length or diameter, respectively.

We can see that the time when the settling fiber starts sliding and departs the fixed fiber delays, i.e. the interaction duration increases, as the fiber aspect ratio increases, no matter whether it is caused by increasing the length or by decreasing the diameter. Nevertheless, the effect caused by varying the diameter is more significant and the delay rate seems higher at a higher aspect ratio, whereas it seems higher at a lower aspect ratio in case of varying the length. Therefore, the fiber aspect ratio $\varphi$ is not an independent parameter for the interaction process.

TABLE IV The time and angle when settling fiber starts sliding along and departs the fixed fiber at different $\varphi$

| $\varphi_l$ | 30 | 35 | 40 | 45 | 50 | 55 | 60 |
|---|---|---|---|---|---|---|---|
| Time of start sliding (s) | 4.61 | 5.15 | 5.60 | 6.04 | 6.49 | 6.94 | 7.37 |
| Time of departing fixed fiber (s) | 17.68 | 19.18 | 20.09 | 20.99 | 21.85 | 22.70 | 23.52 |
| Angle of departing fixed fiber (°) | 82.49 | 82.03 | 81.40 | 80.79 | 80.21 | 79.68 | 79.20 |
| $\varphi_r$ | 30 | 35 | 40 | 45 | 50 | 55 | 60 |
| Time of start sliding (s) | 3.69 | 4.80 | 5.96 | 7.25 | 8.66 | 10.18 | 11.80 |
| Time of departing fixed fiber (s) | 12.64 | 17.31 | 22.11 | 27.50 | 33.44 | 39.94 | 46.98 |
| Angle of departing fixed fiber (°) | 80.46 | 81.43 | 81.96 | 82.34 | 82.65 | 82.91 | 83.13 |

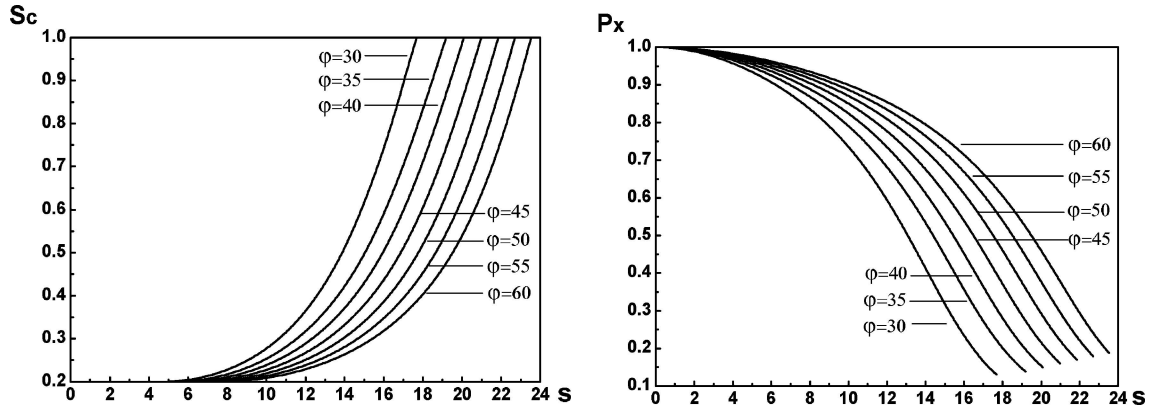


*Figure 11* Results for different fiber aspect ratios by changing the fiber length only.

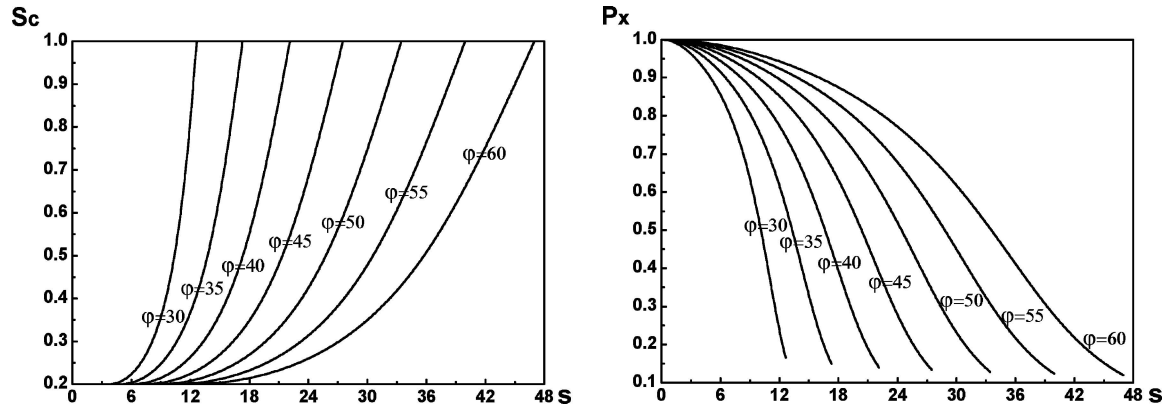


*Figure 12* Results for different fiber aspect ratios by changing the fiber diameter only.

## 3.6. Effect of solvent viscosity on the interaction process

The results for different solvent viscosities are shown in Fig. 13, in which it can be seen that the settling fiber begins to slide at later time and the interaction duration between settling fiber and fixed fiber increases as the solvent viscosity increases. This is originated from the fact that the increase of solvent viscosity results in the enhancement of viscous drag. The delay time that the settling fiber starts sliding along the fixed fiber and the increase of interaction duration at different solvent viscosity are listed in Table V, in which we can see that for a definite increment of solvent viscosity (5 cSt), the delay time that the settling fiber starts sliding along the fixed fiber is same (1.342 s), and the increase of interaction duration is almost same (around 2.46 s). So the interaction duration is directly proportional to the solvent viscosity.

TABLE V The delay time that settling fiber starts sliding and the increase of interaction duration at different solvent viscosity $\nu$

| $\nu$ (cSt) | 20–25 | 25–30 | 30–35 | 35–40 | 40–45 |
|---|---|---|---|---|---|
| Delay time of start sliding (s) | 1.342 | 1.342 | 1.342 | 1.342 | 1.342 |
| Increase time of interaction duration (s) | 2.47 | 2.46 | 2.46 | 2.45 | 2.45 |

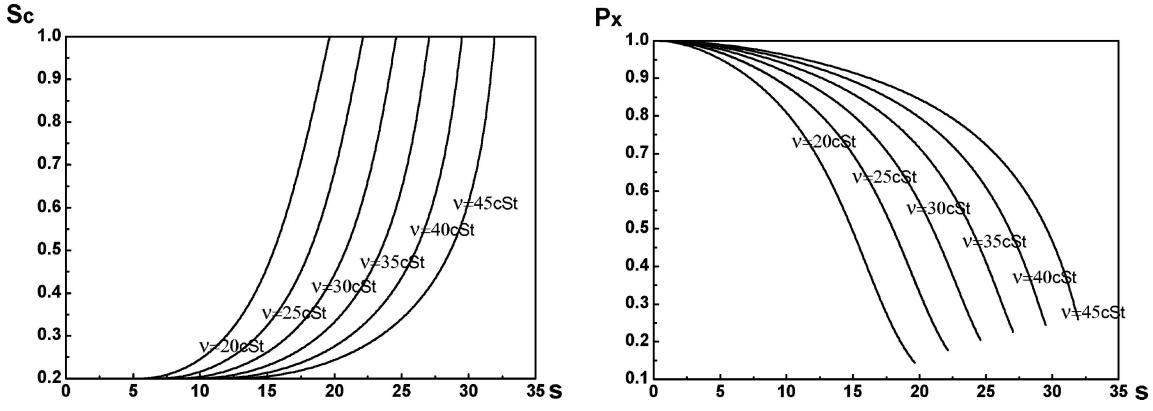


*Figure 13* Results for different solvent viscosities (the unit of $\nu$ is cSt ($10^{-6}$ m$^2$ s$^{-1}$)).

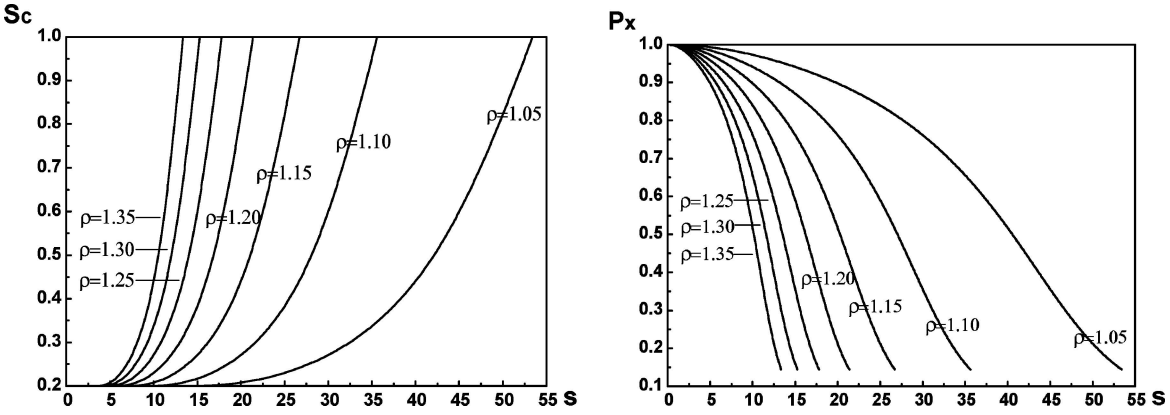


*Figure 14* Results for different fiber specific weight (the unit of $\rho$ is $10^3$ kg/m$^3$ ).

### 3.7. Effect of fiber specific weight on the interaction process

Changing the fiber specific weight, we have the position of contact point and angle between settling fiber axis and horizontal at different time as shown in Fig. 14. Table VI lists the time when settling fiber starts sliding along and departs the fixed fiber at different fiber specific weight, respectively. It shows that the settling fiber begins to slide earlier and departs from the fixed fiber earlier remarkably as the fiber specific weight increases.

### 3.8. The synthetic parameter related to the fiber and the fluid

We have discussed the effects of initial contact point, initial orientation of settling fiber, angle between two fixed fibers, initial angular velocity of settling fiber, fiber aspect ratio, solvent viscosity and fiber specific weight on the interaction process. It is necessary to derive a synthetic parameter $A$ which contains these quantities, allowing the total duration of interaction between the fibers to be expressed as $T = g(A)$. The $\pi$ theorem is used to derive the parameter $A$ in the paper. We take the characteristic quantities which were used in the experiments by Petrich and Koch [8]: half fiber length $l_0 = 1.5$ mm, radius $R_0 = 40$ $\mu$m, specific weight $\rho_0 = 1.222 \times 10^3$ kg/m$^3$, solvent viscosity $\nu_0 = 20\ cSt$, initial contact point $S_0 = 0.05$, initial orientation of settling fiber $\theta_0 = 10^\circ$ and angle between two fixed fibers $\phi_0 = 20^\circ$. Non-dimensionlizing $l$, $R$, $\rho$, $\nu$, $S_0$, $\theta_0$ and $\phi$ by the characteristic quantities, we have $l' = l/l_0$, $R' = R/R_0$, $\rho' = \rho/\rho_0$, $\nu' = \nu/\nu_0$, $S_0' = S_c/S_0$, $\theta_0' = \theta/\theta_0$ and $\phi' = \phi/\phi_0$ as shown in Tables VII–XIII.

From Table VII, we can see that the time when settling fiber starts sliding along and departs the fixed fiber changes linearly with $\nu'$. Therefore, we assume

$$A = \frac{\nu' l'^{\alpha} \phi'^{\varsigma}}{R'^{\beta} \rho'^{\gamma} S_0'^{\delta} \theta_0'^{\lambda}} \tag{9}$$

Similarly we can calculate the undetermined constant $\alpha, \beta, \gamma, \delta, \lambda, \varsigma$ from Tables VIII–XIII by using $\pi$ theorem. Finally we have

$$A = \frac{\nu' l'^{0.701}}{R'^{3.21} \rho'^{8.87} S_0'^{0.27} \theta_0'^{1.355} \phi'^{0.005}} \tag{10}$$

TABLE VI The time when settling fiber starts sliding along and departs the fixed fiber at fiber specific weight $\rho$

| $\rho$($10^3$ kg/m$^3$) | 1.05 | 1.10 | 1.15 | 1.20 | 1.25 | 1.30 | 1.35 |
|---|---|---|---|---|---|---|---|
| Time of start sliding (s) | 14.60 | 9.74 | 7.30 | 5.84 | 4.87 | 4.17 | 3.65 |
| Time of departing fixed fiber (s) | 53.42 | 35.62 | 26.70 | 21.37 | 17.81 | 15.26 | 13.35 |

TABLE VIIA The case of different solvent viscosity $\nu'$

| $\nu'$ | 1.00 | 1.25 | 1.5 | 1.75 | 2.00 | 2.25 |
|---|---|---|---|---|---|---|
| Time of start sliding (s) | 5.369 | 6.711 | 8.053 | 9.395 | 10.737 | 12.079 |
| Time of departing fixed fiber (s) | 19.67 | 22.14 | 24.60 | 27.06 | 29.51 | 31.86 |

TABLE VIIB The case of different $\Delta\nu'$

| $\Delta\nu'$ | 1.0–1.25 | 1.25–1.5 | 1.5–1.75 | 1.75–2.0 | 2.0–2.25 |
|---|---|---|---|---|---|
| Delay time of start sliding (s) | 1.342 | 1.342 | 1.342 | 1.342 | 1.342 |
| Increase time of interaction duration (s) | 2.47 | 2.46 | 2.46 | 2.45 | 2.45 |

TABLE VIII The case of different angle between two fixed fibers $\phi'$

| $\phi'$ | 0.15 | 0.25 | 0.5 | 0.75 | 1 | 1.25 |
|---|---|---|---|---|---|---|
| Time of departing fixed fiber (s) | 19.75 | 19.70 | 19.64 | 19.56 | 19.53 | 19.54 |
| $\phi'$ | 1.5 | 2.25 | 2.5 | 2.75 | 3 | |
| Time of departing fixed fiber (s) | 19.57 | 19.80 | 19.95 | 20.17 | 20.48 | |

TABLE IX The case of different initial contact point $S_0'$

| $S_0'$ | 1 | 2 | 3 | 4 | 5 | 6 |
|---|---|---|---|---|---|---|
| Time of departing fixed fiber (s) | 44.43 | 29.15 | 23.07 | 19.64 | 17.37 | 15.72 |

TABLE X The case of different initial orientation of settling fiber $\theta_0'$

| $\theta_0'$ | 0 | 1 | 1.5 | 2.0 | 2.5 | 3.0 |
|---|---|---|---|---|---|---|
| Time of departing fixed fiber (s) | 19.64 | 16.89 | 15.48 | 14.05 | 12.74 | 11.60 |

TABLE XI The case of different fiber specific weight $\rho'$

| $\rho'$ | 0.8592 | 0.9002 | 0.9411 | 0.9820 | 1.0229 | 1.0638 | 1.1047 |
|---|---|---|---|---|---|---|---|
| Time of departing fixed fiber (s) | 53.42 | 35.61 | 26.70 | 21.37 | 17.81 | 15.26 | 13.35 |

TABLE XII The case of different half fiber length $l'$

| $l'$ | 0.8 | 0.933 | 1.067 | 1.2 | 1.333 | 1.467 | 1.6 |
|---|---|---|---|---|---|---|---|
| Time of start sliding (s) | 4.61 | 5.15 | 5.60 | 6.04 | 6.49 | 6.94 | 7.37 |
| Time of departing fixed fiber (s) | 17.68 | 19.18 | 20.09 | 20.99 | 21.85 | 22.70 | 23.53 |

TABLE XIII The case of different fiber radius $\boldsymbol{R}'$

| $R'$ | 1.25 | 1.0714 | 0.9375 | 0.8333 | 0.75 | 0.6818 | 0.6250 |
|---|---|---|---|---|---|---|---|
| Time of start sliding (s) | 3.69 | 4.80 | 5.96 | 7.25 | 8.66 | 10.18 | 11.80 |
| Time of departing fixed fiber (s) | 12.64 | 17.31 | 22.11 | 27.50 | 33.44 | 39.94 | 46.98 |

From Equation 10, we can see that the fiber specific weight has the largest, while angle between two fixed fibers has the least effect on the interaction between the fibers.

## 4. Conclusions

The governing equations for the mechanical interactions of three contact fibers in fiber suspensions were solved numerically. The following conclusions can be drawn:

(1) The settling fiber begins to slide at earlier time and the interaction duration between settling fiber and fixed fiber decreases as $S_0$ increases. The angle between settling fiber axis and horizontal becomes large quickly for the situations with large $S_0$. The interaction duration between settling fiber and fixed fiber becomes short with increasing of initial angles between two kinds of fibers. When the initial angles are great 15°–20°, the settling fiber does not pivot about the fixed fiber, while sliding along and rotating the fixed fiber directly. The initial contact point and the initial orientation angle have significant effects on the interaction process of fibers.

(2) The angle $\phi$ between two fixed fibers has an insignificant effect on the process of interaction. When $\phi$ is around 20°, the time when the settling fiber departs from the fixed fiber is the shortest. As $\phi$ is larger than 30° , the time when the settling fiber starts sliding increases obviously. The initial angular velocity of settling fiber has no effect on the position of contact point and the angle between settling fiber axis and horizontal.

(3) The fiber aspect ratio $\varphi$ is not an independent parameter involving in the interaction between the fibers. The interaction duration increases as the fiber aspect ratio increases, however, the effect caused by reducing the diameter is more significant than that caused by increasing the length.

(4) The interaction duration is directly proportional to the solvent viscosity and verse directly to the fiber specific weight remarkably.

(5) A synthetic parameter $A$ which contains the quantities affecting the interaction duration is derived to uniquely describe the total duration of interaction between the fibers. The formulation of $A$ shows that the fiber specific weight has the most important, while angle between two fixed fibers has the least effect on the interaction between the fibers.


## Acknowledgements

The authors are grateful to the National Natural Science Foundation of China (No. 10372090) and the Doctoral Program of Higher Education in China (No. 20030335001) for financial support.


## References


1. R. R. SUNDARAJAKUMAR and D. L. KOCH, *J. Non Newtonian Fluid Mech.* **73** (1997) 205.
2. L. F. CARTER, Ph. D. thesis, University of Michigan, Ann Arbor, MI, 1967.
3. C. P. J. BENNINGTON, R. J. KEREKES and J. R. GRACE, *Can. J. Chem. Eng.* **68** (1990) 748.
4. M. A. ZIRNSAK, D. U. HUR and D. V. BOGER, *J. Non-Newtonian Fluid Mech.* **54** (1994) 153.
5. S. R. ANDERSSON and A. RASMUSON, *J. Pulp Pap. Sci.* **23** (1997) J5.
6. I. LEE, *J. Mater. Sci.* **30** (1995) 6019.
7. S. ZEHG, E. T. KERNS and R. H. DAVIS, *Phys. Fluids.* **8** (1996) 1389.
8. M. P. PETRICH and D. L. KOCH, *Phys. Fluids* **10** (1998) 2111.
9. C. MOHEND and D. L. KOCH, *J. Rheology*, **45** (2001) 369.
10. J. Z. LIN, Z. C. ZHANG and Z. S YU, *J. Mater. Sci.* **38** (7) (2003) 1499.
11. G. X. BATCHELOR, *J. Fluid Mech* **44** (1970) 419.
12. M. B. MACKAPLOW and E. S. G. SHAQFEH, *J. Fluid Mech* **329** (1996) 155.



*Received 18 August*
*and accepted 11 November 2004*